The Astrophysical Journal Letters, 841:L26 (6pp), 2017 June 1 https://doi.org/10.3847/2041-8213/aa72da

The Hottest Hot Jupiters May Host Atmospheric Dynamos

T. M. Rogers[1,2] and J. N. McElwaine[2,3]
[1] Department of Mathematics and Statistics, Newcastle University, Newcastle upon Tyne, UK
[2] Planetary Science Institute, Tucson, AZ 85721, USA
[3] Department of Earth Sciences, Durham University, Durham, UK
Received 2016 November 20; revised 2017 April 28; accepted 2017 May 12; published 2017 May 26

Abstract

Hot Jupiters have proven themselves to be a rich class of exoplanets that test our theories of planetary evolution and atmospheric dynamics under extreme conditions. Here, we present three-dimensional magnetohydrodynamic simulations and analytic results that demonstrate that a dynamo can be maintained in the thin, stably stratified atmosphere of a hot Jupiter, independent of the presumed deep-seated dynamo. This dynamo is maintained by conductivity variations arising from strong asymmetric heating from the planets' host star. The presence of a dynamo significantly increases the surface magnetic field strength and alters the overall planetary magnetic field geometry, possibly affecting star–planet magnetic interactions.

Key words: dynamo – magnetohydrodynamics (MHD) – planets and satellites: gaseous planets

1. Introduction

To date, more than 5000 exoplanets have been discovered and a couple hundred are considered "hot Jupiters"—Jupiter-sized planets close to their host star. Hot Jupiters were the first detected exoplanets and remain the best characterized due to their favorable observing conditions. Because of their close proximity to their host star, these planets are tidally locked with a constant dayside and nightside. This asymmetric heating leads to strong eastward-directed atmospheric winds that have been studied extensively (Showman & Guillot 2002; Cho et al. 2003; Cooper & Showman 2005; Dobbs-Dixon & Lin 2008; Showman et al. 2009; Lewis et al. 2010; Rauscher & Menou 2010; Thrastarson & Cho 2010; Heng et al. 2011; Kataria et al. 2016). While atmospheric dynamic calculations generally yield similar results, such as eastward winds in excess of a km s^{-1}, observations indicate varying circulation efficiency. Infrared observations have demonstrated that hot Jupiters have a range of day–night temperature differentials, and there is some indication that this variation is temperature dependent, with hotter planets showing larger differentials than cooler planets (Cowan & Agol 2011; Komacek & Shomwan 2016).

Intense irradiation from the host star can lead to thermal ionization of several alkali metals (Batygin & Stevenson 2010; Perna et al. 2010a). Therefore, hot Jupiters are partially ionized. Numerous authors have demonstrated that this ionization allows atmospheric winds to couple to the deep-seated, dynamo-driven magnetic field (Batygin & Stevenson 2010; Perna et al. 2010a, 2010b; Menou 2012a). This coupling could lead to currents which penetrate into the deep atmosphere, generating Ohmic heating, which could in turn, contribute to the inflated radii observed in half of all hot Jupiters (Batygin et al. 2011; Wu & Lithwick 2013; Ginzburg & Sari 2015, 2016). Magnetic interaction could also reduce circulation efficiency, particularly in hot planets where the day–night flow could be impeded by the Lorentz force. These results demonstrate that magnetism in hot Jupiters could have important observational consequences, and thus warrant further investigation.

Rogers & Showman (2014) carried out the fist magneto-hydrodynamic (MHD) simulations of a hot Jupiter that self-consistently included Ohmic heating. Those simulations found that inclusion of magnetic fields could severely affect the atmospheric flows leading to variable and reversed winds. They also found that while the MHD simulations did reproduce the qualitative picture proposed by earlier theoretical work (Menou 2012a; Rauscher & Menou 2013), they failed to reproduce the amplitude of Ohmic heating required to explain inflated radii (Rogers & Komacek 2014; Rogers & Showman 2014). The discrepancy between theoretical models and numerical simulations leaves the viability of the Ohmic mechanism for inflating exoplanets still in question.

Hot Jupiters also likely interact with their host stars' magnetic field, possibly leading to observable features such as asymmetry in the light curves of transiting planets (Vidotto et al. 2010; Cauley 2015) and induced activity in the atmosphere of their host star (Shkolnik et al. 2003, 2005). Such interactions depend on the planetary magnetic field strength and geometry (Cuntz et al. 2000; Ip et al. 2004). Therefore, understanding the planetary magnetic field is important if we are to correctly interpret such observations.

The day–night temperature differential on hot Jupiters leads to severe day–night variations in ionization and, hence, conductivity. Similarly, there are large variations in conductivity between deep and shallow atmospheric layers. Busse & Wicht (1992) showed that variations in conductivity in the direction of the dominant flow could lead to a dynamo. More recently, Petrelis et al. (2016) showed that a temperature-dependent conductivity could produce a dynamo, even with small temperature fluctuations and a weakly temperature-dependent conductivity. Hot Jupiter atmospheres are perhaps the most asymmetric astrophysical objects, with perhaps the largest temperature (conductivity) variations and so provide an ideal testbed of the theories outlined in those works. Here, we present three-dimensional (3D) numerical simulations and analytic results that show that a variable conductivity dynamo (VCD) may proceed in some hot Jupiter atmospheres.

2. Numerical Simulations of Atmospheric Dynamos

We solve the full MHD equations in 3D in the anelastic approximation, as described in Rogers & Komacek (2014). The

model solves the following equations:

$$\boldsymbol{\nabla} \cdot \bar{\rho}\boldsymbol{v} = 0, \tag{1}$$

$$\boldsymbol{\nabla} \cdot \boldsymbol{B} = 0, \tag{2}$$

$$\bar{\rho}\frac{\partial \boldsymbol{v}}{\partial t} + \boldsymbol{\nabla} \cdot (\bar{\rho}\boldsymbol{v}\boldsymbol{v}) = -\boldsymbol{\nabla} p - \rho \bar{g}\hat{\boldsymbol{r}} + 2\bar{\rho}\boldsymbol{v} \times \boldsymbol{\Omega} + \ldots + \boldsymbol{\nabla} \cdot \left[2\bar{\rho}\bar{\nu}\left(e_{ij} - \frac{1}{3}\delta_{ij}(\boldsymbol{\nabla} \cdot \boldsymbol{v})\right)\right] - \frac{1}{\mu_0}\boldsymbol{B} \times (\boldsymbol{\nabla} \times \boldsymbol{B}), \tag{3}$$

$$\frac{\partial T}{\partial t} + (\boldsymbol{v} \cdot \nabla)T = -v_r\left[\frac{\partial \overline{T}}{\partial r} - (\gamma - 1)\overline{T}h_\rho\right] + (\gamma - 1)Th_\rho v_r + \ldots + \gamma\overline{\kappa}\left[\nabla^2 T + (h_\rho + h_\kappa)\frac{\partial T}{\partial r}\right] + \frac{T_{\rm eq} - T}{\tau_{\rm rad}} + \frac{\eta}{\mu_o \rho c_p}|\nabla \times \boldsymbol{B}|^2. \tag{4}$$

Equation (1) represents the continuity equation in the anelastic approximation (Gough 1969; Rogers & Glatzmaier 2005). This approximation allows some level of compressibility by allowing variation of the reference state density, $\bar{\rho}$, which varies in this model by four orders of magnitude. Equation (2) represents the conservation of magnetic flux. Equation (3) represents conservation of momentum including Coriolis and Lorentz forces. Equation (4) represents the energy equation including a forcing term to mimic stellar insolation (fourth term on the right-hand side, RHS) and Ohmic heating (fifth term on the RHS, where $T_{\rm eq}$ is defined in Equation (6)). All variables take their usual meaning, and details can be found in Rogers & Komacek (2014).

In the work presented here, the magnetic diffusivity η (inverse conductivity) is a function of all space. Therefore, the magnetic induction equation is

$$\frac{\partial \boldsymbol{B}}{\partial t} = \nabla \times (\boldsymbol{v} \times \boldsymbol{B}) + \eta\nabla^2\boldsymbol{B} - (\nabla\eta) \times (\nabla \times \boldsymbol{B}). \tag{5}$$

In the hot Jupiter system, toroidal field can be generated from poloidal field by radial shear due to stronger winds at the planetary surface. Although the dynamo mechanism by conductivity variations is subtle, one can show that given the correct alignment between $\nabla \times \boldsymbol{B}$ and $\nabla\eta$, the last term on the RHS of Equation (5) can provide a positive α effect, thus regenerating poloidal field from toroidal and closing the dynamo loop.

The magnetic diffusivity is calculated from the initial temperature profile given by

$$T_{\rm eq}(r, \theta, \phi) = \overline{T}(r) + \Delta T_{\rm eq}(r)\cos\theta\cos\phi, \tag{6}$$

where $\overline{T}(r)$ is the reference state temperature from Rogers & Komacek (2014) and $\Delta T_{\rm eq}$ is the specified day–night temperature, which is extrapolated logarithmically from the surface to 10 Bar. Using this temperature profile, the magnetic diffusivity is calculated using the method from Rauscher & Menou (2013):

$$\eta(r, \theta, \phi) = 230\frac{\sqrt{T_{\rm eq}}}{\chi_e} \tag{7}$$

and χ_e is the ionization fraction. The ionization fraction is calculated at each point using the Saha equation taking into account all elements from hydrogen to nickel and abundances from Lodders (2010).

The fiducial numerical model we present is Model M8 from Rogers & Komacek (2014), but with $\Delta T_{\rm eq} = 1000$ K, such that the nightside at the top of the domain is ~1800 K and the dayside is ~2800 K. The atmospheric winds found in the hydrodynamic model are shown in Figure 1. Near the surface, where the temperature forcing is strong, the model produces strong eastward-directed jets at low latitudes, return flows at high latitudes, and weaker, hemispheric meridional circulation. Deeper in the atmosphere, the forcing is reduced and winds fall off dramatically with depth. Radial flows are extremely weak throughout, with amplitudes 0.1%–1% of their horizontal counterparts. These winds are similar to those found in many other hydrodynamical simulations of hot Jupiters (Cooper & Showman 2005), with the main difference being that our winds are slightly weaker, probably due to the use of the full viscous term, rather than using a hyperdiffusivity.

Magnetic effects are then investigated by including an initial magnetic field of 5 G at the bottom and 3 G at the top of the domain. Figure 2 shows the magnetic diffusivity as a function of radius for various latitudes and longitudes for our model. This "dynamo" model has no continuously imposed field, unlike the models presented in Rogers & Showman (2014) and Rogers & Komacek (2014). However, to fully investigate the effect of an atmospheric dynamo, we ran three additional models: (1) "constant η"—a model with a constant magnetic diffusivity equal to the mean diffusivity (5×10^{11}), (2) "imposed+dynamo"—a model with variable conductivity, as shown in Figure 2 but with an imposed dipolar magnetic field of strength 3 G at the base of the simulated domain meant to mimic the deep-seated, convectively driven dynamo, and (3) "imposed+constant"—a model with an imposed dipolar magnetic field of strength 3 G at the base of the simulated domain, but with a constant magnetic diffusivity (5×10^{11}).

The magnetic diffusivity is *not* a function of time in any of the models. That is, it does not change due to advection of heat or Ohmic heating. We will include this effect in forthcoming papers, but discuss the possible relevance of a fully temperature-dependent conductivity in Section 5.

3. Numerical Results

The effect of the magnetic field on the atmospheric winds depends sensitively on the diffusivity profile and strength of the magnetic field, details of which can be found in Rogers & Komacek (2014). In the dynamo model presented here, the atmospheric winds are strongly coupled to the magnetic field, and therefore the winds become weaker and variable. A time snapshot of magnetic field lines for the "dynamo" model is shown in Figure 3. The top row shows magnetic field lines looking onto the terminator[4], color-coded by the azimuthal field strength, with blue positive and magenta negative. Magnetic field is swept from the dayside, where field and flow are strongly coupled, to the nightside, where much of this field is dissipated. The collision between the strongly coupled field on the dayside and the weakly coupled field on the nightside leads to complex field topology and magnetic energy generation. This interaction in particular generates strong latitudinal field at the terminator, as can be seen in Figure 3(d).

[4] The terminator is the transition between day–night side; here, we are referring to the terminator eastward of the substellar point.

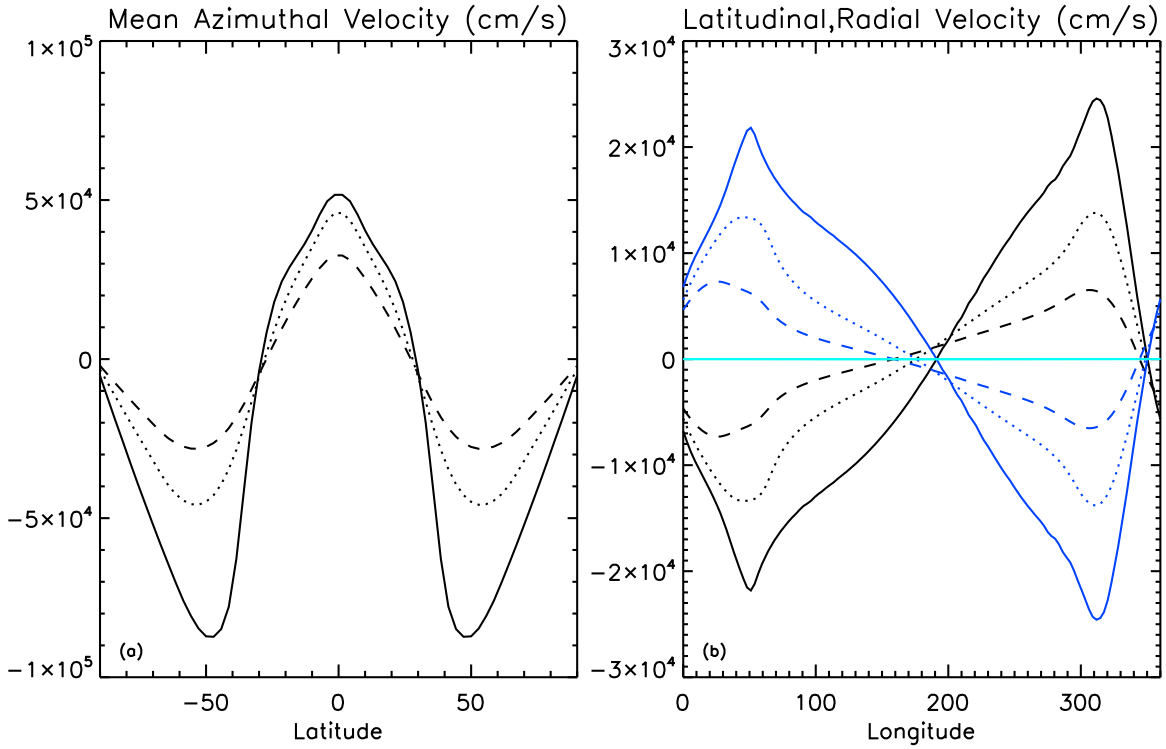

Figure 1. Atmospheric winds in hot Jupiter atmosphere. (a) Time and longitudinally averaged longitudinal velocity at the surface (solid line), 95% (dotted line), and 85% of the computed domain (dashed line). (b) Latitudinal velocity averaged in time and over the northern/southern hemispheres (blue/black lines, respectively) at the same depths as (a). Similarly averaged radial velocities are shown in cyan.

Investigation of (5), shows that the VCD α effect is $\propto \boldsymbol{J} \times \boldsymbol{\nabla}\eta$. The current, $\boldsymbol{J}$, is strongly correlated with vorticity, which tends to be strongest at the day–night terminator and on the nightside (Rogers & Komacek 2014). The terminator is also where conductivity gradients are large; hence, in this region, the necessary conditions for a dynamo are satisfied. Specifically, we find that the radial component of the magnetic field is regenerated predominantly from the azimuthal diffusivity gradient $\sim\boldsymbol{\nabla}\eta_\phi J_\theta$ and the latitudinal component is regenerated predominantly from the radial diffusivity gradient $\sim\boldsymbol{\nabla}\eta_r J_\phi$. The azimuthal component of the magnetic field is regenerated by *both* the typical Ω effect and by radial gradients in magnetic diffusivity, $\sim\boldsymbol{\nabla}\eta_r J_\theta$. The presence of a dynamo is confirmed in Figure 4, which shows the ratio of the magnetic to kinetic energy as a function of time for the "dynamo model" (solid line) and the "constant η" model (dashed–dotted line drops so precipitously it can barely be seen in bottom left corner).

In the saturated state, the magnetic energy generation is balanced with Ohmic heating, which we also show in Figure 4. If we compare the Ohmic heating here to the values obtained in Rogers & Komacek (2014) for a 3 G imposed field (see their Table 1), we see that the Ohmic heating here is equivalent to the Ohmic heating in a cooler model (between M6b3 and M7b3). Therefore, we conclude that the presence of a horizontally varying conductivity and the dynamo it produces result in slightly *lower* overall Ohmic heating than one would expect from a model that does not consider a horizontally varying conductivity. This is likely because magnetic energy is maintaining the VCD, rather than being dissipated.

The bottom row of Figure 3 shows the extrapolated field lines (out to $2R_p$) for this model. There we see that the magnetic field is very asymmetric, with poloidal field concentrated predominantly on the dayside of the planet. Near the equator, the surface poloidal field (defined as $B_p = \sqrt{B_\theta^2 + B_r^2}$) is $\sim$15 G on the dayside of the planet and 7 G on the nightside of the planet. These values are 16 G/8 G for the "imposed+dynamo" model and $\sim$1 G on both the dayside and nightside for the "imposed+constant" model. The inclusion of conductivity variations significantly increases the surface planetary field strength and leads to a highly asymmetric field. Therefore, unless the internal, convectively driven, magnetic field is particularly strong (in excess of 15 G at the surface), the surface planetary magnetic field is likely dominated by the magnetic field generated in the atmosphere, at least in hotter hot Jupiters.

The asymmetry in the field persists to $2R_p$ where about 65% of the magnetic energy is found in the dipole component, 25% is in the $l = 2$, $m = 1$ component and 10% in the $l = 3$, $m = 2$ component, although by $4R_p$ the dipole component represents 95% of the total energy. However, these percentages fluctuate significantly in time. Such a complex field structure in space and time likely affects the SPMI expected in these close-in systems (Cuntz et al. 2000; Ip et al. 2004; Strugarek et al. 2015).

4. Analytic Models of Dynamo Behavior in a Hot Jupiter

The flow profile and conductivity variations in hot Jupiters are relatively simple; therefore, we attempt to solve this system analytically. While the diffusivity and initial velocity vary on a large scale in a hot Jupiter atmosphere, the magnetic energy is generated in a narrow region near the terminator. In that region, the length scale of velocity and diffusivity variations is small. Therefore, we apply the standard technique of multiple scales from homogenization theory (Mei & Vernescu 2010) in 3D Cartesian coordinates. This is a method for deriving an

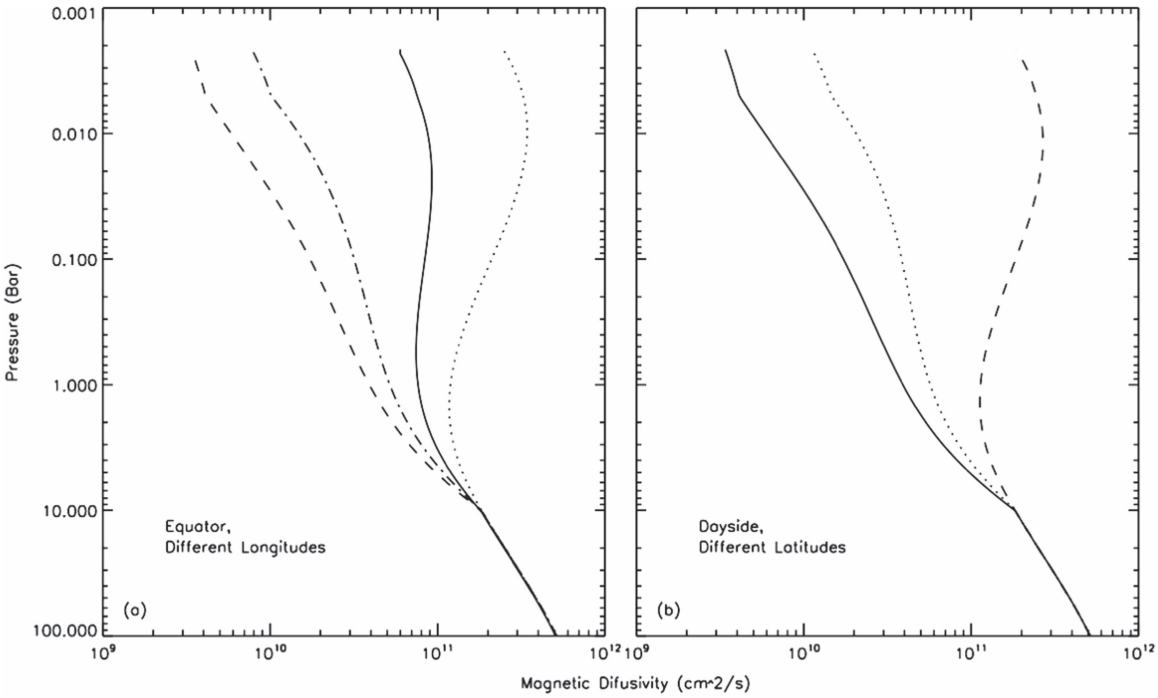

Figure 2. Profile of magnetic diffusivity as a function of longitude (a) and latitude (b). (a) Radial profile of diffusivity at the equator at the substellar point (dashed line), the nightside (dotted line), near the terminator (dashed–dotted line), and the mean (solid line). (b) Radial profile of diffusivity at the substellar point at the equator (solid line), mid-latitude (dotted line) and near the pole (dashed line).

equation for the large-scale variations in the magnetic field by averaging over the periodic small-scale variations. We assume that the conductivity and velocity vary on a small spatial scale defined by a large wavenumber k and define $\boldsymbol{X} = (X, Y, Z) = k\boldsymbol{x}$ and all functions must be periodic in $\boldsymbol{X}$. We then look for a solution of the form

$$\boldsymbol{B} = \boldsymbol{B}_0(t, \boldsymbol{x}) + k^{-1}\boldsymbol{B}_1(t, \boldsymbol{x}, \boldsymbol{X}) + k^{-2}\boldsymbol{B}_2(t, \boldsymbol{x}, \boldsymbol{X}) + \cdots. \quad (8)$$

When we substitute (8) into (5), we get a series of equations at each order in k. The leading order equation, $O(k^1)$, gives an equation for $\boldsymbol{B}_1$ in terms of $\boldsymbol{B}_0$, and the $O(k^0)$ equation, after averaging over the periodic cell, gives an equation for $\boldsymbol{B}_0$. The $\boldsymbol{B}_1$ equation is

$$\nabla' \times [(\eta(\nabla \times \boldsymbol{B}_0 + \nabla' \times \boldsymbol{B}_1) - \boldsymbol{v} \times \boldsymbol{B}_0] = 0, \quad (9)$$

where $\nabla' = (\partial_X, \partial_Y, \partial_Z)$. This is to be contrasted with (4) in Petrelis et al. (2016), where there is no spatial variation in η and a time derivative is included. We then write $\eta = \eta_0(1 + \delta\eta')$, where η_0 is constant, and η' varies between ± 1; thus, δ controls the strength of the variation in conductivity. Writing $\boldsymbol{B}_1 = \sum_{k=0} \delta^k \boldsymbol{C}_k$ and Taylor expanding $(1 + \delta\eta')^{-1}$, we get a series of Poisson equations for C_k that can be easily solved to give $\boldsymbol{B}_1$ in terms of $\boldsymbol{B}_0$ and $(\nabla \times \boldsymbol{B}_0)$. This expansion is convergent for $\delta < 1$, which we also expect on physical grounds since this corresponds to positive diffusivity everywhere.

We choose profiles similar to those found in hot Jupiters. Assuming $\hat{\boldsymbol{x}}$, $\hat{\boldsymbol{y}}$, and $\hat{\boldsymbol{z}}$ correspond to the azimuthal, latitudinal, and radial directions, we write

$$\eta' = \cos Z \sin X \sin Y, \quad (10)$$

and

$$\boldsymbol{v} = \sin Z(\hat{\boldsymbol{x}} U \sin X \cos Y + \hat{\boldsymbol{y}} V \cos X \sin Y). \quad (11)$$

Here, U and V represent the azimuthal and meridional velocity amplitude, respectively (in the case that $U + V = 0$, this is the same as Petrelis et al. 2016). As discussed in Section 3, the winds in the hot Jupiter atmosphere are largely two-dimensional and are reasonably described by (11). Using the method described above, we solve for $\boldsymbol{B}_1$ to $O(\delta^4)$ and the $\boldsymbol{B}_0$ equation becomes

$$\frac{\partial \boldsymbol{B}_0}{\partial t} = \eta_0\left[1 - \frac{\delta^2}{12} - \frac{\delta^4}{72}\right]\nabla^2 \boldsymbol{B}_0 + \eta_0 \frac{\delta}{24} \times \left[1 + \frac{\delta^2}{6} + \frac{233881}{3852288}\delta^4\right]\nabla \times \boldsymbol{B}_0' + O(\delta^6), \quad (12)$$

where $\boldsymbol{B}_0' = -VB_x\hat{\boldsymbol{x}} + UB_y\hat{\boldsymbol{y}} + (U - V)B_z\hat{\boldsymbol{z}}$. The $\nabla \times \boldsymbol{B}_0'$ term gives rise to the dynamo effect. When $UV > V^2$ (which is the appropriate case for hot Jupiters), the large-scale magnetic field is unstable in the $\hat{\boldsymbol{x}}$ direction and the minimum critical Reynolds number, defined as UL/η where L is the length scale of the large-scale magnetic field, is[5]

$$R_{\rm mc} > \frac{\sqrt{1 + \sqrt{2}}\,(6 - \delta^2)(12 + \delta^2)}{\delta\left(6 + \delta^2 + \frac{233881}{642048}\delta^4\right)}. \quad (13)$$

In hot Jupiters, the day–night diffusivity, $\eta_{\rm max}/\eta_{\rm min} = (1 + \delta)/(1 - \delta)$, varies between $\sim 10^1$ and 10^4, which corresponds to a δ between 0.9 and 0.999. Figure 5 shows the approximate convergence of $R_{\rm mc}(\delta)$ as δ approaches 1. If we take $\delta = 0.9$, the $R_{\rm mc}$ needed for instability is ~ 14. Using the length scale over which magnetic energy is generated at the terminator ($\sim 10^{10}$ cm) and a typical velocity of $\sim 10^4$ cm s^{-1},

[5] This stability condition is dependent on the exact diffusivity and velocity profile. While many profiles give instability, many do not, and we are still in the process of finding a generalized solution to the conditions for instability.

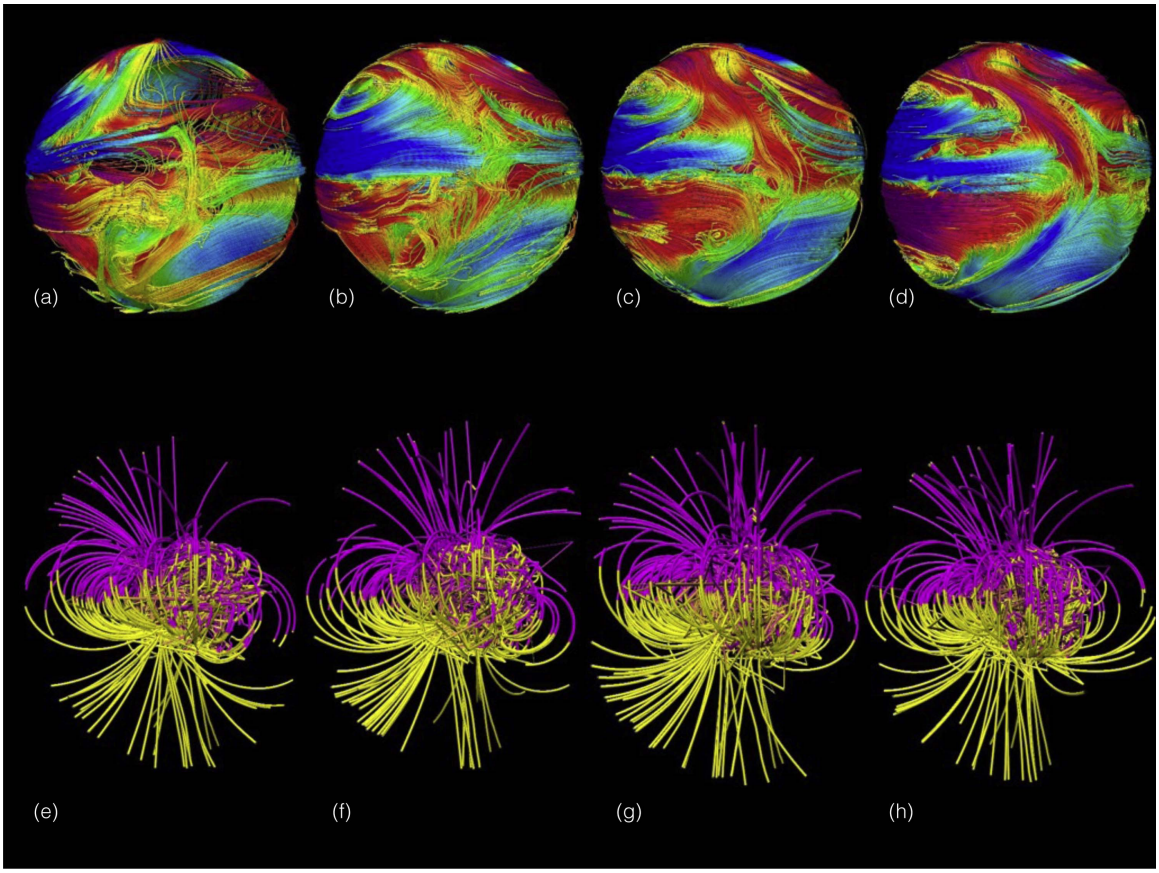

Figure 3. Time snapshots of toroidal (azimuthal) magnetic field (looking onto the terminator) ((a)–(d)) and the radial magnetic field ((e)–(h)).

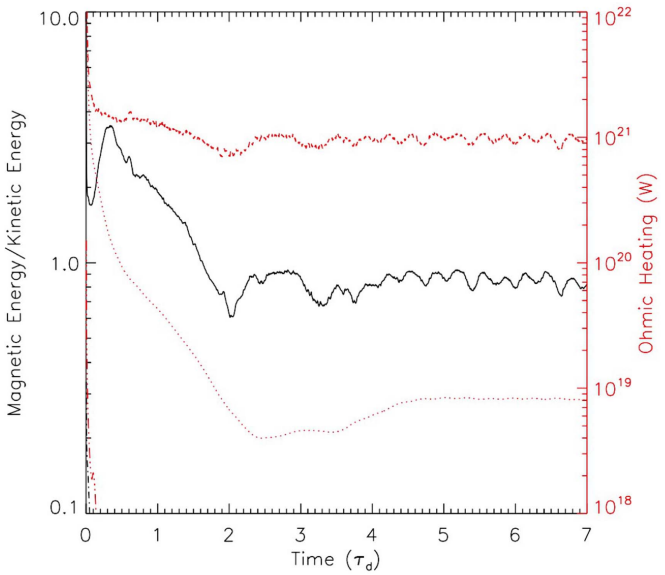

Figure 4. Magnetic energy and Ohmic heating as a function of time, displayed in diffusion times, using the mean diffusivity 10^{11} cm^2 s^{-1}. The left-hand axis shows the ratio of magnetic to kinetic energy (solid black line), clearly showing a dynamo as the magnetic energy is maintained against diffusion. The right-hand axis shows Ohmic heating integrated below 10 Bar (dotted line) and over the whole layer (dashed line).

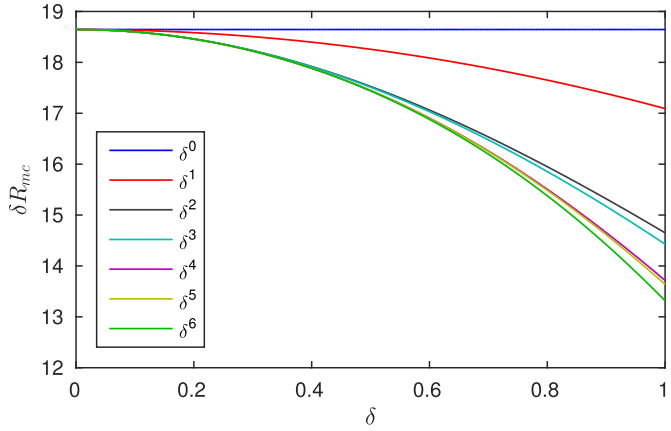

Figure 5. Scaled critical magnetic Reynolds number $\delta R_{\rm mc}$ as a function of δ for different accuracies of $\boldsymbol{B}_1$ solution.

we conclude that in order for a hot Jupiter atmosphere to host a dynamo, the nightside magnetic diffusivity must be $\lesssim 10^{12}$–10^{13} cm^2 s^{-1}, or a temperature of roughly 1400 K on the *nightside* of the planet. We expect the estimate for the diffusivity could vary by about an order of magnitude due to variations in metallicity and the inclusion of a temperature-dependent diffusivity. Therefore, we conclude that a VCD only occurs in the hotter hot Jupiter atmospheres.

5. Discussion

Using numerical simulations coupled with analytic results, we have shown that hot Jupiters with nightside temperatures that are above ∼1400 K could host dynamos driven by spatial

conductivity variations due to asymmetric heating from the host star. Lower temperatures and weak day–night temperature differentials do not produce dynamos. This is remarkable, not just because the dynamo is driven by conductivity variations (as has been shown previously), but also because it is maintained in a stably stratified, thin atmosphere. The inclusion of horizontal variations in conductivity reduces Ohmic heating compared to a similar temperature object with no such variations. However, it is hard to make a direct comparison because of the large conductivity variations. To really investigate Ohmic heating, the analysis presented here will have to be done for a host of planetary temperatures and day–night temperature differences, something that is currently underway. Moreover, one needs to include the recovered Ohmic heating in a planetary evolution model to make a more concrete statement about the viability of Ohmic heating in explaining hot Jupiter radii. Finally, we will have to consider the interaction of the atmospheric field with the convectively generated field.

Whatever the deep-seated field, it will be subject to interaction with the atmospheric winds and the variable conductivity in the atmosphere, both of which affect the overall field strength and geometry. We find that unless the deep-seated dynamo magnetic field is unreasonably strong; the surface planetary magnetic field strength is dominated by the *induced* field, particularly on the dayside of the planet. We also find that the magnetic field geometry is asymmetric, with dayside fields approximately two times larger than their nightsides (dependent on the day–night temperature difference). Furthermore, we find that the energy in the dipole component of the magnetic field varies substantially in time. All of these factors affect star–planet magnetic interactions (Strugarek et al. 2015) and the inferences we make from such interactions (Vidotto et al. 2010).

While we have made progress by including a spatially dependent conductivity, we have yet to consider a *temperature-dependent* conductivity. We expect this will play an important role, possibly leading to the instability proposed by Menou (2012b) and likely increasing the overall Ohmic heating and altering further still the magnetic structure. Such simulations will be the subject of a forthcoming paper.

Support for this research was provided by NASA grant NNX13AG80G to T.R. Computing was carried out on Pleiades at NASA Ames. T.R. thanks Graeme Sarson, Gary Glatzmaier, and Chris Jones for useful conversations leading to the development of this manuscript.

References

Batygin, K., Stevenson, D., & Bodenheimer, P. 2011, ApJ, 738, 1
Batygin, K., & Stevenson, D. J. 2010, ApJL, 714, L238
Busse, F., & Wicht, J. 1992, GApFD, 64, 135
Cauley, W. 2015, ApJ, 810, 13
Cho, J. Y.-K., Menou, K., Hansen, B., & Seager, S. 2003, ApJL, 587, 117
Cooper, C. S., & Showman, A. P. 2005, ApJL, 629, L45
Cowan, N. B., & Agol, E. 2011, ApJ, 729, 54
Cowan, N. B., Machalek, P., Croll, B., et al. 2012, ApJ, 747, 82
Cuntz, M., Saar, S., & Musielak, Z. 2000, ApJL, 533, L151
Demory, B., & Seager, S. 2011, ApJS, 197, 12
Dobbs-Dixon, I., & Lin, D. N. C. 2008, ApJ, 673, 513
Ginzburg, S., & Sari, R. 2015, ApJ, 803, 111
Ginzburg, S., & Sari, R. 2016, ApJ, 819, 116
Gough, D. O. 1969, JAtS, 26, 448
Heng, K., Menou, K., & Phillipps, P. J. 2011, MNRAS, 413, 2380
Huang, X., & Cumming, A. 2012, ApJ, 757, 47
Ip, W., Kopp, A., & Hu, J. 2004, ApJL, 602, L53
Kataria, T., Sing, D., Lewis, N., et al. 2016, ApJ, 821, 9
Knutson, H. A., Charbonneau, D., Allen, L. E., et al. 2007, Natur, 447, 183
Knutson, H. A., Charbonneau, D., Cowan, N. B., et al. 2009, ApJ, 703, 769
Komacek, T., & Showman, A. 2016, ApJ, 821, 26
Laughlin, G., Crismani, M., & Adams, F. C. 2011, ApJL, 729, L7
Lewis, N. K., Showman, A. P., Fortney, J. J., et al. 2010, ApJ, 720, 344
Lodders, K. 2010, Principles and Perspectives in Cosmochemistry (Berlin: Springer)
Mei, C. C., & Vernescu, B. 2010, Homogenization Methods for Multiscale Mechanics (Singapore: World Scientific)
Menou, K. 2012a, ApJ, 745, 138
Menou, K. 2012b, ApJL, 754, L9
Perna, R., Menou, K., & Rauscher, E. 2010a, ApJ, 719, 1421
Perna, R., Menou, K., & Rauscher, E. 2010b, ApJ, 724, 313
Petrelis, F., Alexakis, A., & Gissinger, C. 2016, PhRvL, 116, 161102
Rauscher, E., & Menou, K. 2010, ApJ, 714, 1334
Rauscher, E., & Menou, K. 2013, ApJ, 764, 103
Rogers, T. M., & Glatzmaier, G. A. 2005, ApJ, 620, 432
Rogers, T. M., & Komacek, T. 2014, ApJ, 794, 132
Rogers, T. M., & Showman, A. P. 2014, ApJL, 782, L4
Shkolnik, E., Bohlender, D., Walker, G., & Collier-Cameron, A. 2005, ApJ, 676, 628
Shkolnik, E., Walker, G., & Bolender, D. 2003, ApJ, 597, 1092
Showman, A. P., Fortney, J. J., Lian, Y., et al. 2009, ApJ, 699, 564
Showman, A. P., & Guillot, T. 2002, A&A, 385, 166
Strugarek, A., Brun, A., Matt, S., & Reville, V. 2014, ApJ, 795, 86
Strugarek, A., Brun, A., Matt, S., & Reville, V. 2015, ApJ, 815, 111
Thrastarson, H. T., & Cho, J. Y.-K. 2010, ApJ, 716, 144
Vidotto, A., Jardine, M., & Helling, C. 2010, ApJL, 722, 168
Wu, Y., & Lithwick, Y. 2013, ApJ, 763, 13